Scientific Contributions Oil & Gas, Vol. 47. No. 2, August: 131-142

SCIENTIFIC CONTRIBUTIONS OIL AND GAS
Testing Center for Oil and Gas
LEMIGAS

Journal Homepage:http://www.journal.lemigas.esdm.go.id
ISSN: 2089-3361, e-ISSN: 2541-0520

Seismic Data Processing and Seismic Inversion in The Ray Parameter Domain: Common Reflection Point (CRP) Stack and Ray Impedance

Wahyu Triyoso[1], Edycakra Immanuel Sinaga[2] and Madaniya Oktariena[2]

[1]Global Geophysics Group, Institut Teknologi Bandung
Ganesha Street No.10, Bandung, 40132, Indonesia

[2]Department of Geophysical Engineering, Faculty of Mining and Petroleum Engineering, Institut Teknologi Bandung
Ganesha Street No.10, Bandung, 40132, Indonesia

Corresponding author: wtriyoso@gmail.com

Manuscript received: June 24th, 2024; Revised: July 24th, 2024
Approved: July 30th, 2024; Available online: August 22th, 2024

ABSTRACT - Reservoir characterization can be enhanced by integrating lateral and vertical perspectives from seismic surveys and well logging, respectively. Seismic impedance is a crucial parameter, calculated by multiplying the rock density by the primary (P) wave velocity. While acoustic impedance solely considers these two factors, elastic impedance incorporates additional angular measurements and secondary (S) wave velocity data. Elastic impedance, however, equates the incident angle with the transmission angle in disregard of Snell's law; therefore, it provides a simplified representation of seismic impedance. This study explores an alternative approach to seismic impedance, known as ray impedance. We calculated ray impedance by tracing the impedance variation along the path of a seismic ray, considering its changing velocity and angle as it traveled through different subsurface strata. We transformed the seismic information from the offset space to the ray parameter space, to achieve ray parameter stacking. Unlike the traditional angle domain inversion, which uses near-angle, mid-angle, and far-angle seismic stack data, the ray-impedance inversion utilized segments of ray data: near-ray, mid-ray, and far-ray. We compared the common depth point stack, ray stack, and angle stack methods to infer the acoustic, elastic, and ray impedance characteristics. Challenges with gas cloud interference in seismic data imaging were present. We developed a ray parameter strategy to address these imaging difficulties. The comparison of different stacking techniques indicated that ray stacking could offer an alternative for imaging in the presence of gas cloud effects. Furthermore, impedance cross-plotting demonstrated that ray impedance provided a more discernible separation of low-clay-content zones than elastic impedance did. Overall, data processing in the ray parameter domain yielded positive imaging outcomes in the presence of gas clouds, suggesting that ray impedance is a practical method for lithological differentiation.

Keywords: acoustic impedance, elastic impedance, ray impedance.

How to cite this article:

Wahyu Triyoso, Edycakra Immanuel Sinaga and Madaniya Oktariena, 2024, Seismic Data Processing and Seismic Inversion in The Ray Parameter Domain: Common Reflection Point (CRP) Stack and Ray Impedance, Scientific Contributions Oil and Gas, 47 (2) pp. 131-142. DOI.org/10.29017/SCOG.47.2.1621.

INTRODUCTION

The geoscientific investigation of subsurface structures, such as horizons and faults, often involves qualitative methods to outline the geometry of these structures. Nonetheless, quantitative approaches are vital for the comprehensive understanding of subsurface layers. These approaches rely on numerical data derived from inverted seismic recordings.

Seismic impedance, which indicates how well a layer transmits seismic waves, is a crucial piece of these quantitative data. Seismic impedance is a critical property directly related to reflectivity. For reservoir characterization, seismic inversion is an important method for formulating subsurface models. Seismic inversion integrates seismic and well-log data to predict structures in the Earth's subsurface, (Tarantola 2005). The choice of the impedance log input is pivotal for enhancing the accuracy of seismic impedance estimates in the inversion process.

There are two main types of seismic impedance: acoustic (AI) and elastic (EI). The AI is calculated by multiplying the density of a given layer with its P-wave velocity, assuming that the waves meet the layer at a perpendicular angle and neglecting the S-wave velocity effects. The EI, on the other hand, extends the calculation to nonzero incidence angles, as proposed by (Connolly 1999). The EI inversion method has been successfully applied to characterize many hydrocarbon reservoirs (Connolly 1999; Avseth 2005). This method, based on the Zoeppritz equation (Aki & Richard 1980), also takes into account S-wave velocity data. The EI is calculated by applying a consistent angle value to represent both the incident and transmission angles. This approach, however, overlooks Snell's law, which states that the angles of incidence and transmission differ because of the variable media through which the wave travels.

Although the EI is often more accurate than the AI, its reliability can be undermined by two key assumptions: the use of a fixed angle value for both the incident and transmitted angles, which overlooks Snell's law, and the adoption of a constant K value, which poses challenges owing to the instability that can arise from different K inputs in the EI approximation.Ray impedance (RI), presents a more precise approach. It utilizes inputs similar to those used for the calculation of EI, such as P- and S-wave velocity and density; yet its calculation does not rely on a singular angle value, but incorporates a p-parameter ray value to better account for wave path variations. Building on (Wang 1999) approach to reflectivity approximation (Wang 2017), the concept of RI was used to estimate the seismic impedance along specific ray paths under Snell's law. In contrast to the use of fixed angles (as in the EI), the RI is based on a constant ray path, meaning that different subsurface media result in different ray angles. The RI approach has been shown to aid lithological discrimination (Lu 2010; Zhang 2010).

In this study, we applied the concept of RI to process seismic data in the ray parameter domain as a solution to the presence of subsurface gas clouds that cause poor seismic data imaging.

METHODOLOGY

Data

This study incorporated the synthetic elastic model simulation developed by (Triyoso et al. 2018). This model, based on actual log data, includes a genuine seismic processing velocity model that highlights the location of the gas cloud, as depicted in Figure 1.

The P-wave velocity model for a seismic line crossing a specific well included the correlation between density and the P-wave velocity, derived from the well log data. The results of the correlation analysis were used to develop a low-frequency model of the subsurface.

Following (Triyoso et al. 2017, 2018), the recording configuration used split-spread shooting with 153 shot points, 161 geophone groups spaced 25 m apart, and a 50-meter interval between sources, to produce the seismic shot gather model.

Elastic Impedance and Ray Impedance

Snell's Law describes the relationship between the angle of incidence and the angle of transmission (measured from the normal line) of the ray path that passes through different media boundaries (Figure 2).

Snell's Law is expressed mathematically by the following equation:

$$p_1 = p_2 = \frac{sin\theta_1}{\alpha_1} = \frac{sin\theta_2}{\alpha_2}, \quad (1)$$

where p_1 is the ray parameter of medium 1, p_2 is the ray parameter of Medium 2, θ_1 the angle of the incidence with P-wave velocity, and θ_2 is the angle of transmission in Medium 2 with P-wave velocity.

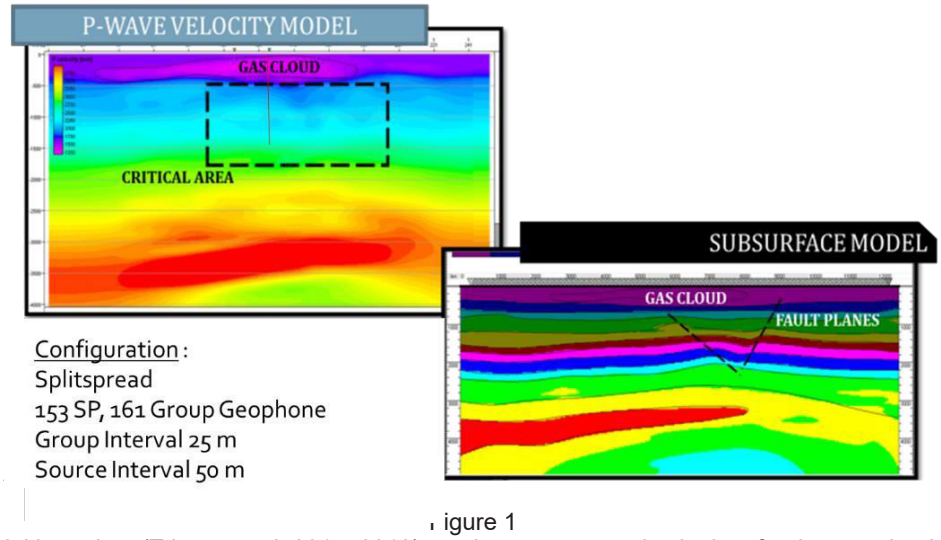

, igure 1
The data model based on (Triyoso et al. 2017, 2018) used to construct seismic data for the gas cloud scenario. Full wave modeling was applied to produce seismic data gatherings.

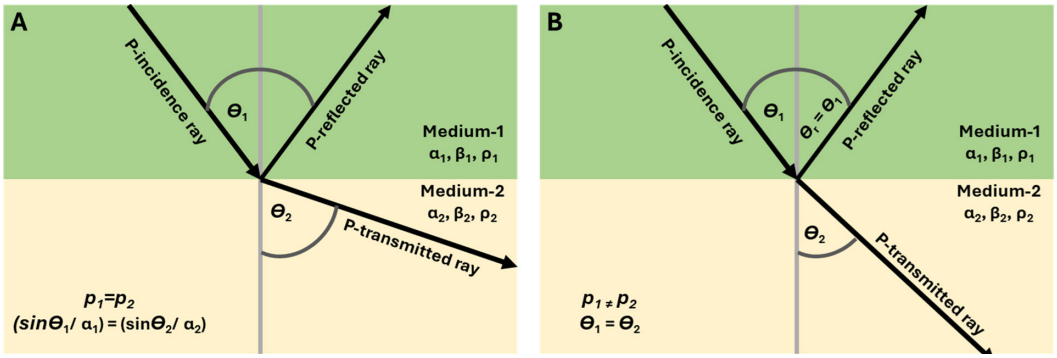

Figure 2
Seismic reflection and transmission according to (a) Snell's Law and (b) assumption in elastic impedance.

The seismic impedance can be defined as the product of velocity and density, which are typically estimated from post-stack seismic data. The AI is the seismic impedance for a zero angle of incidence. Its mathematical expression is as follows:

$$AI = \rho\alpha, \tag{2}$$

where ρ is the density and α is the P-wave velocity. The EI is the seismic impedance for a non-zero angle of incidence. Its mathematical expression is as follows (Connolly 1999):

$$EI = \rho^{(1-4Ksin^2\theta)}\alpha^{(1-tan^2\theta)}\beta^{(-8Ksin^2\theta)} \tag{3}$$

where ρ is the density, α is the P-wave velocity, β is the S-wave velocity, θ is the angle of incidence, and K is a substitution assumed to be of constant value. For $\theta = 0$, the EI equals the AI.

Figure 3, illustrating the difference between the constant offset constant angle, and constant rays, explains the basic concept of the ray domain. The constant offset (Figure 3a) shows a seismic ray acquired from the same offset distance. The constant angle (Figure 3b) shows a seismic trace obtained from the same angle. The constant ray (Figure 3c) shows a seismic trace from the same ray. The constant offset condition shows a limited angle value, as seen from the shrinking angle with increasing depth. For a constant angle, the maximum angle value depends on the offset distance in the data. These two approaches are interconnected: a constant offset has a limited angle range, and a constant angle has a limited offset range. Meanwhile, the constant ray condition demonstrates that the input of a given angle value is not binding because the ray parameters in different subsurface layers provide different velocity and angle information.

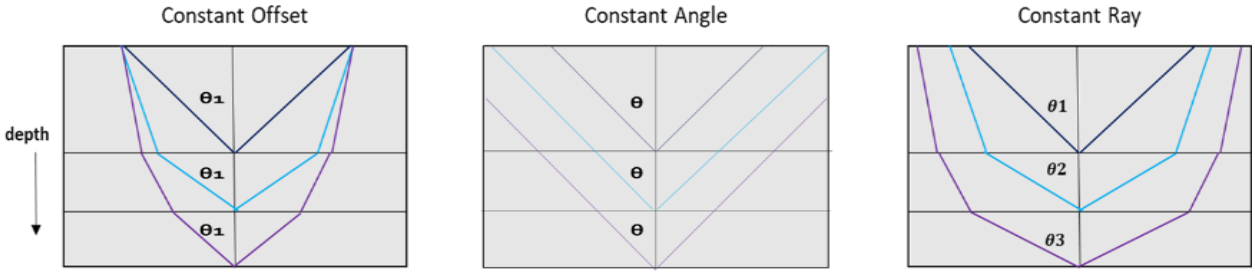

Figure 3
Constant offset (left), constant angle (middle), constant ray (right).

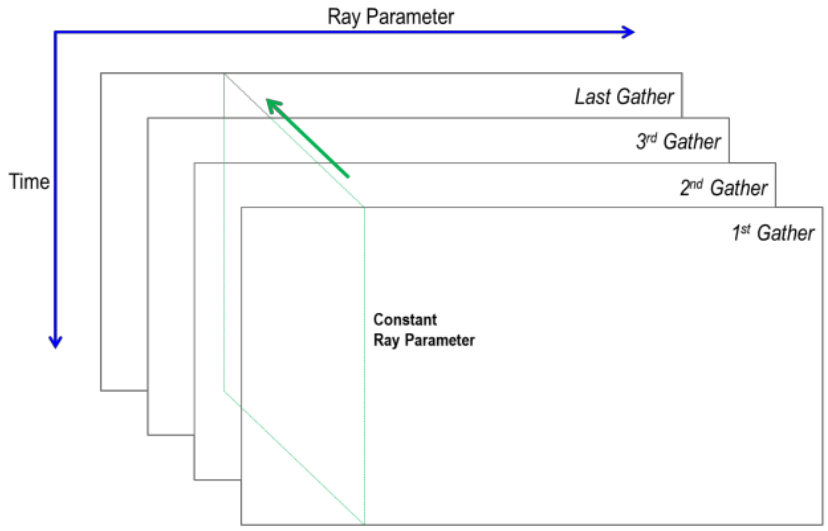

Figure 4
Construction of seismic stack in the constant ray parameter domain.

Mathematically, the RI is the product of density, P-wave velocity, and S-wave velocity; therefore, the RI is a generalization of the AI and EI. The distinguishing factor is that the EI uses one input angle value as a reference for the angles of incidence and transmission, while the RI eliminates this assumption by using ray parameters as the input data.

Wang (1999) introduced the RI equation as follows:

$$RI = \rho\alpha \frac{1}{\sqrt{1-\alpha^2 p^2}} (1-\beta^2 p^2)^{2\left(\left(\frac{\frac{\Delta\rho}{\rho}}{\frac{\Delta\beta}{\beta}}\right)+2\right)}, \quad (4)$$

where ρ is the density, α is the P-wave velocity, β is the S-wave velocity, and p is the constant ray parameter. When = 0, the RI equals the AI.

A further advantage of the RI is that it maintains the dimensionality of the impedance as a direct multiplication product of velocity and density, unlike EI, which has a constantly changing dimensionality owing to its angle of incidence. Following (Wang 1999), it is possible to use a range of angle values, including a wide angle, depending on the signal quality of the angle gather. In this study, however, the quality of data for angles larger than 30° was poor. For this reason, we selected a maximum angle of 30°.

Transformation into the Ray Parameter Domain

The transformation from the time-offset (t-x) to the time-ray (τ-p) domain is based on the following equation:

$$\tau = t - px, \quad (5)$$

where τ is the intercept time, t is the arrival time, p is the ray parameter, and x is the offset

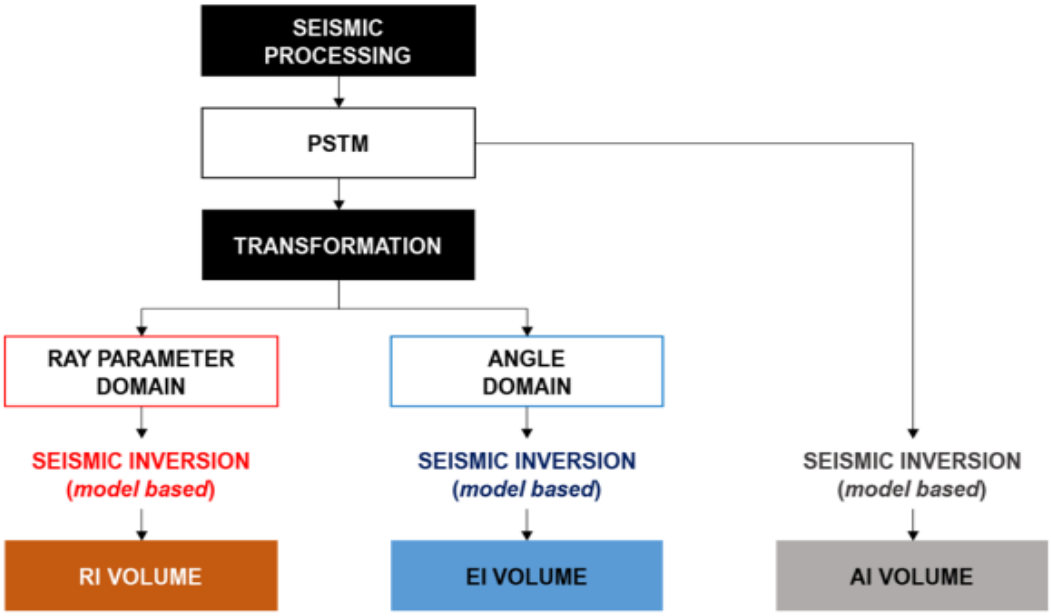

Figure 5
General workflow of this research.

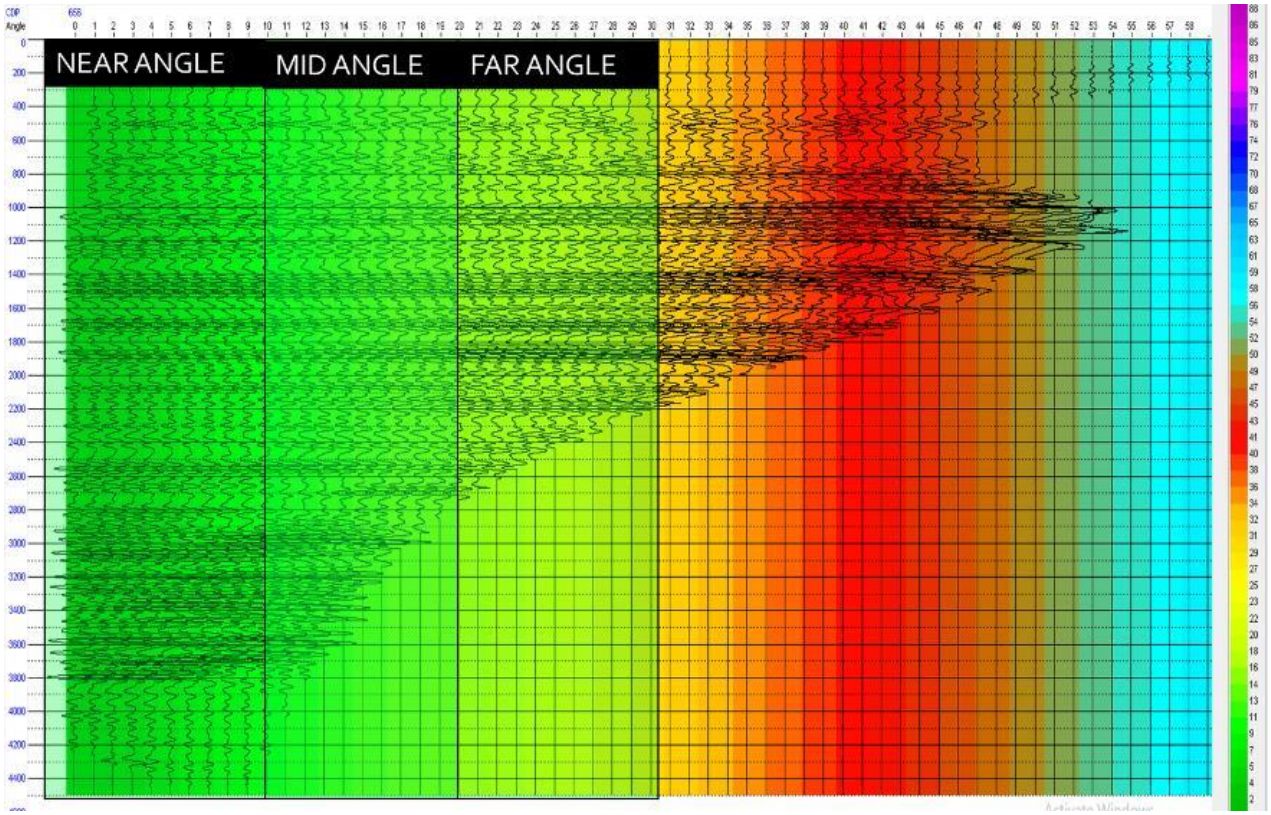

Figure 6
Angle range of the data.

The τ–p transformation process involves the conversion of seismic data from the offset to the ray-parameter domain. We performed this conversion by sorting the seismic data according to ray and then stacking the data corresponding to the same ray to obtain ray stack data. We converted the data to the angle domain using AVO Analysis (Rutherford & Williams 1989), determined the angle value used to construct the angle stack, and then sorted the angle values for each common depth point (CDP) gather. Finally, we performed stacking to obtain the angle stack of the desired angle value, as shown in Figure 4.

The workflow of this study (Figure 5) followed (Sinaga et al. 2018) and (Triyoso et al. 2020, 2023). The seismic data were processed up to the prestack time migration (PSTM) stage. The results of the PSTM gather were converted into a ray-parameter and an angle domain. The ray and angle Stacks were categorized as near, mid, and far. The resulting datasets were then used to generate inverted volumes for the RI, EI, and AI.

Seismic Processing

The processing of the seismic data involved the assignment of a geometry, removal of noise, analysis of velocity, and true amplitude recovery (TAR). The PSTM was then used for data migration. The migrated data were deemed final and converted into the ray and angle domains.

Angle and Ray Value Selection

After examination of the angle range of the data (Figure 6), we set the maximum angle range at 30°. The near, mid-, and far angle was 0–10°, 10–20°, and 20–30°, respectively. We then calculated the ray parameter as the angle counterpart. First, we calculated the average value of the wave velocity P (= 2341). Then, we used the formula to obtain the near ray (0–74 ms/km), mid ray (74–146 ms/km), and far ray (146–191 ms/km).

RESULT AND DISCUSSION

Stack Results

The mid- and far-ray stacks revealed reflectors in the gas cloud zone, as shown in Figure 7. The near ray was still affected by fluid influence from the gas cloud zone, while the mid and far ray were not affected by the gas cloud. The data in the angle domain remained relatively unchanged, and the reflector was slightly strengthened at the far angle. However, data with a more extended offset are needed to obtain an ultra-far angle, which could resemble the mid- and far-ray results.

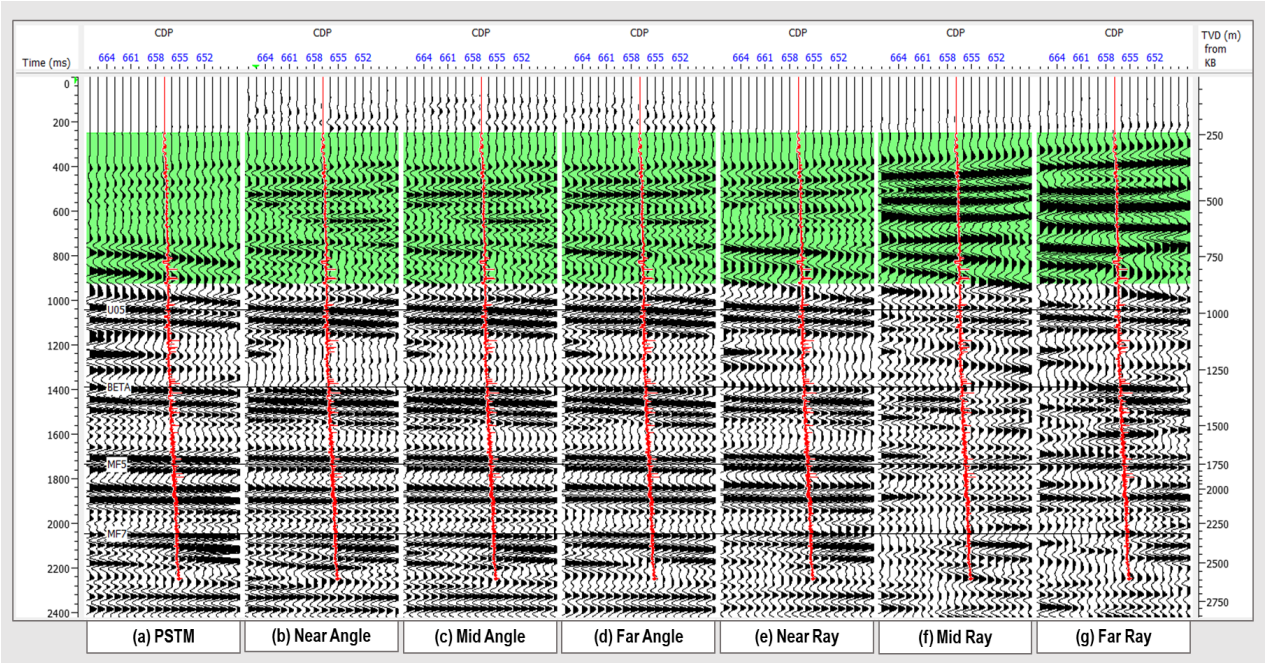

Figure 7
Comparison of the seismic images: (a) PSTM stack, (b) Near-angle stack, (c) Mid-angle stack, (d) Far-angle stack, (e) Near-ray stack, (f) Mid-ray stack, and (g) Far-ray stack.

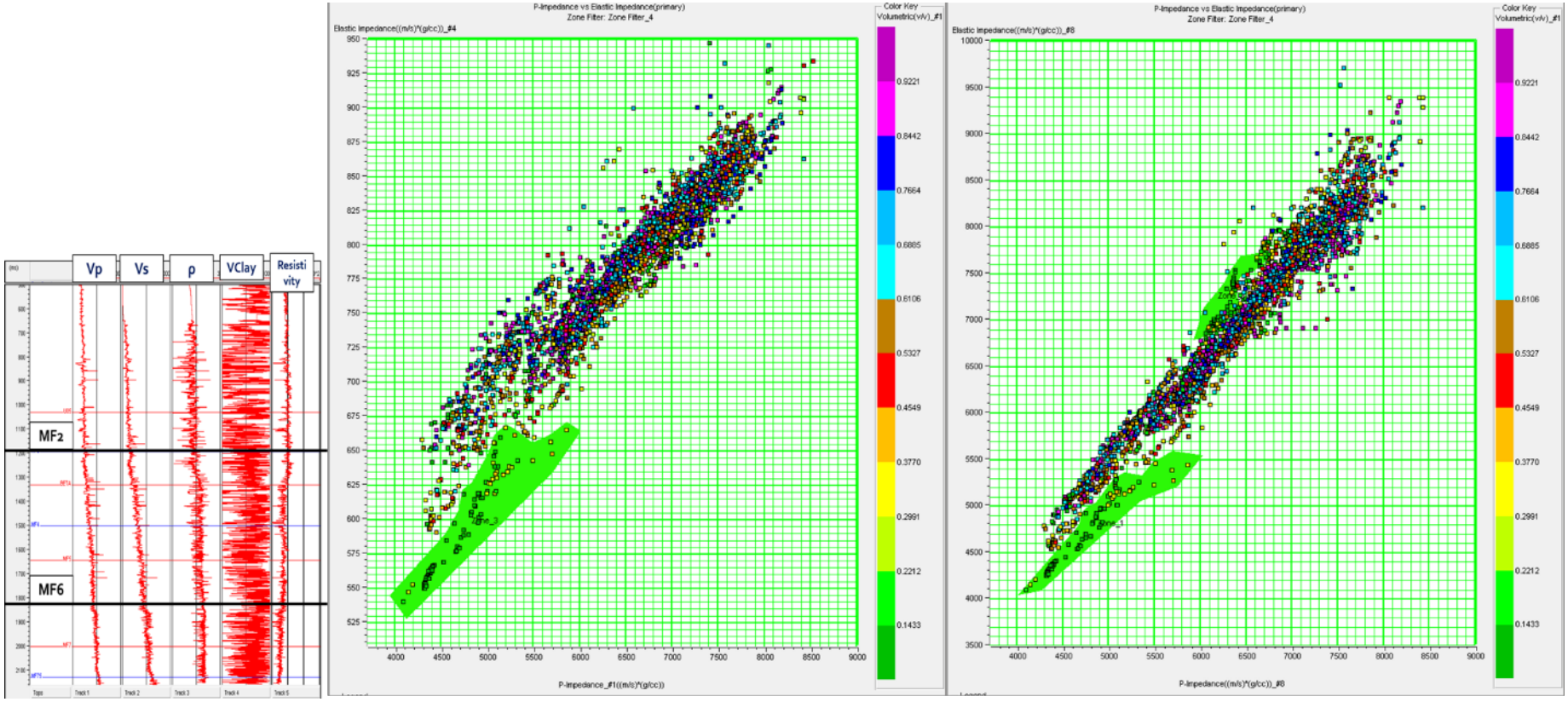

Figure 8
Resolution of low-V clay in AI–EI FAR (left) and AI–RI FAR (right).

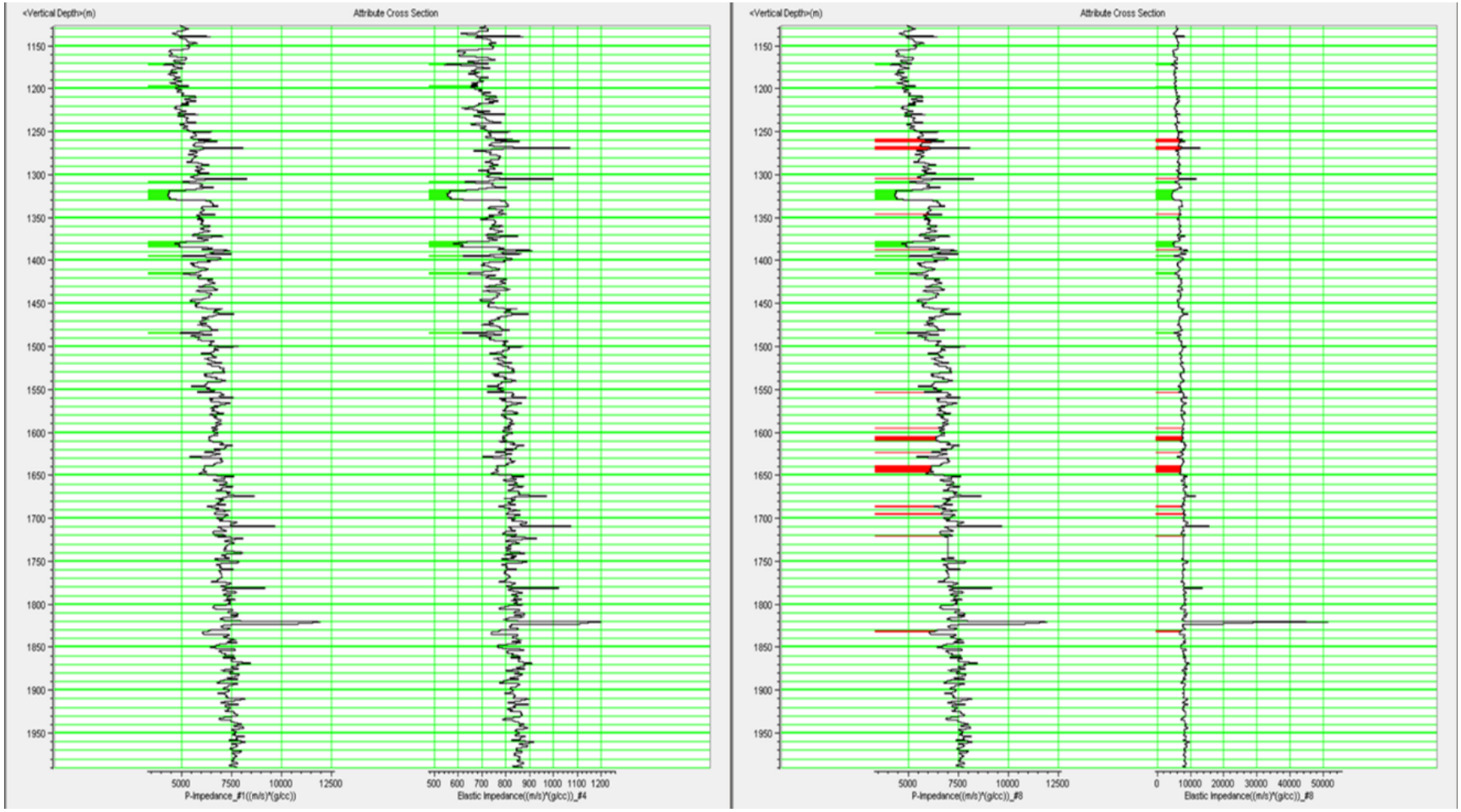

Figure 9
Comparison between AI–EI and AI–RI (cross-sections). The AI–EI results were also evident in the AI–RI (green Zone). The low-V clay with high resistivity (red zone) was resolved clearly using AI–RI, but not AI–EI.

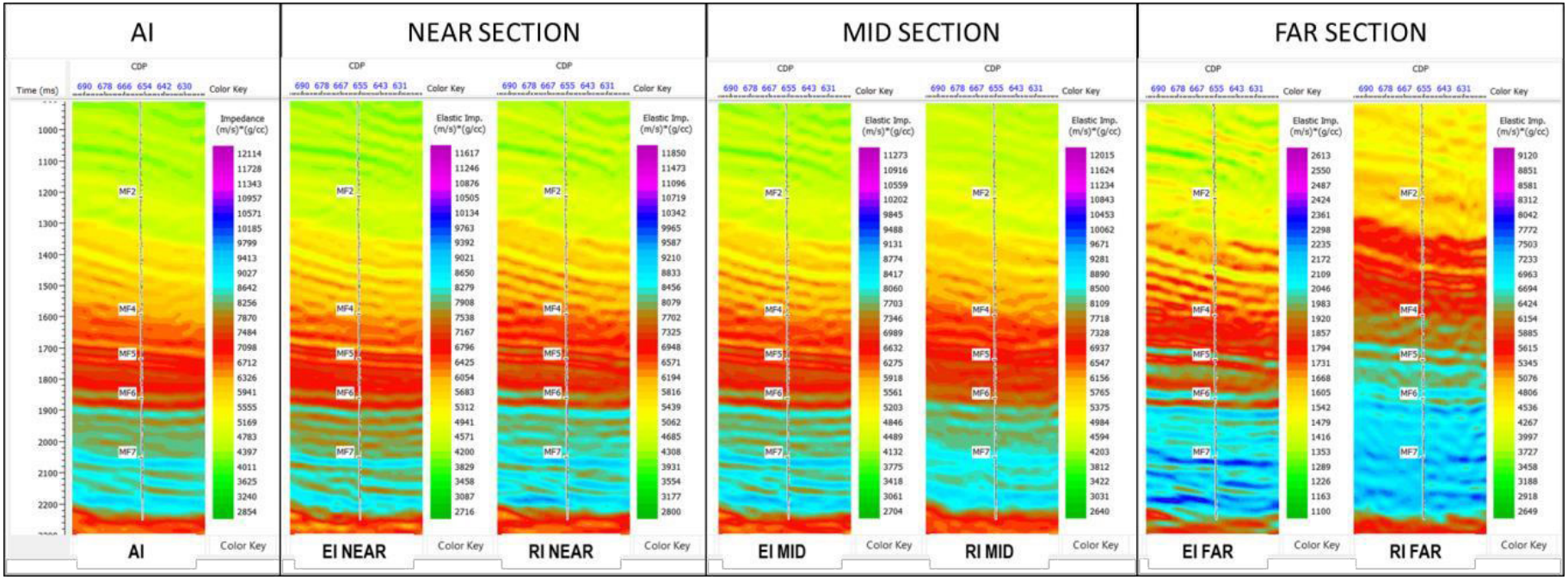

Figure 10
Comparison between the inverted RI and EI volume.

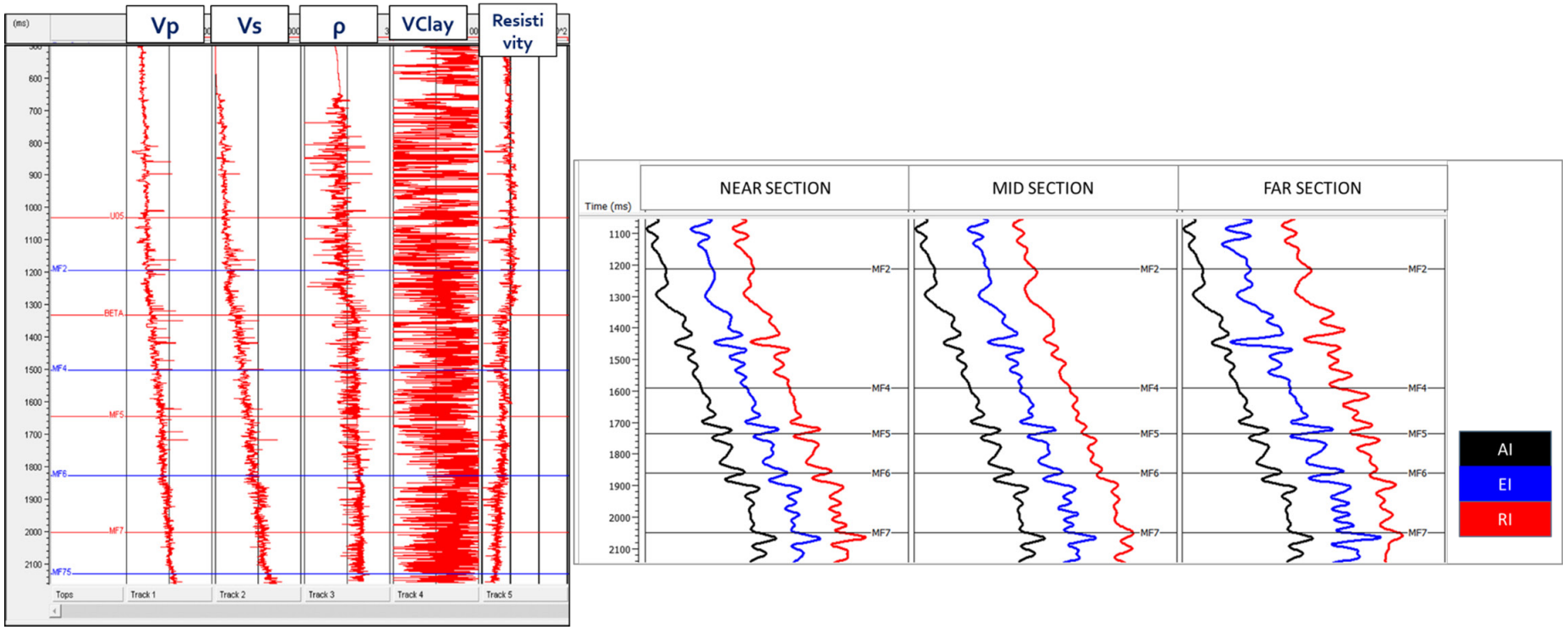

Figure 11
Comparison of the traces of well position extracted from the inverted RI and EI. The inverted RI far-ray stack had a sufficient resolution, and accurately delineated the position of the geological markers.

Zoning Analysis of The Impedance Log

The AI–RI zoning showed a better separation of the low-V clay than the AI–EI zoning (Figure 8). Figure 9 shows that the location of the low-V clay zone was reveled in both the EI and RI. The cross section also revealed the location of the low-V, high-resistivity clay zone (red color in Figure 10).

Seismic Inversion

The seismic inversion results (Figure 10) revealed that the properties of the inverted RI were similar to those of the inverted EI, notwithstanding the disparities between the EI and RI noted in the previous section. A trace of the well location was extracted from each inverted impedance volume to compare the results of the two methods, as shown in Figure 11.

The near and mid sections demonstrated the similarities between the EI and RI. In the far section, the inverted RI had a sufficient resolution, and accurately delineated the geological markers.

CONCLUSION

This study demonstrates the effectiveness of the Ray Impedance (RI) as a viable alternative to Elastic Impedance for seismic imaging, particularly in gas cloud zones. RI successfully revealed the gas cloud zone reflector and provided superior resolution of the low-velocity clay zone compared to EI. Furthermore, AI-RI effectively identified dry-gas sand presence. While both methods showed comparable inversion volumes, AI-RI provided clearer delineation of the low-V clay zone at the well location. The study highlights the capability of RI, especially mid-to-far ray stacks, in revealing the continuation of gas clouds.

ACKNOWLEDGEMENT

We want to thank the Global Geophysics Group, Geophysics Engineering Department, FTTM-ITB Bandung. We also gratefully acknowledge TOTAL E&P Indonesie, Balikpapan – Kalimantan Timur (2015) and LAPI ITB, who assisted with the collection of the well data used to develop the synthetic model.

GLOSSARY OF TERMS

Symbol	Definition	Unit
AI	Acoustic impedance	
EI	Elastic impedance	
RI	Ray impedance	
τ-p	Tau-P	
TAR	True amplitude recovery	
PSTM	Pre-stack Time Migration	
AVO	Amplitude versus offset	
CDP	Common depth point	

REFERENCES

Aki, K. & Richards, P.G., 1980, Quantitative seismology: theory and methods: W.H. Freeman.

Avseth, P., T. Mukerji & G. Mavko, 2005, Quantitative seismic interpretation: Cambridge University Press.

Connolly, P., 1999, Elastic impedance: The Leading Edge, 18, 438-452. https://doi.org/10.1190/1.1438307.

Lu, X., 2010, Seismic Ray Impedance Inversion, 23- 50, a Thesis: Imperial College London.

Rutherford, S.R. & R.H. Williams, 1989, Amplitude-versus-offset variations in gas sands: Geophysics, 54, 680–688. https://doi.org/10.1190/1.1442696.

Sinaga, E., Triyoso, W. & Oktariena, M., 2018, Comparative Study of Seismic Impedance in Ray Parameter Domain: Case Study of Seismic Imaging and Seismic Inversion in Gas Cloud Zone, Proceedings of the 13th SEGJ International Symposium, 2018.

Tarantola, A., 1986, A strategy for nonlinear elastic inversion of seismic reflection data: Geophysics, 51, 1893-1903. https://doi.org/10.1190/1.1442046.

Triyoso, W., Oktariena, M., Sinaga, E. & Syaifuddin, F., 2017, Full Waveform Modelling for Subsurface Characterization with Converted-Wave Seismic Reflection, IOP Conference Series: Earth and Environmental Science, 62. DOI 10.1088/1755-1315/318/1/012035.

Triyoso, W., Oktariena, M. & Muhtar, L.K., 2018, Ray-Binning Angle Stack Domain in Enhancing the Robustness of Converted-Wave Seismic Joint Inversion, Scientific Contributions Oil and Gas Vol. 41, No 3, 2018. DOI: https://doi.org/10.29017/SCOG.41.3.330.

Triyoso, W., Irawan, J. B., Viony, N. C. & Fatkhan, 2020, Application of ZO-CRS Stack on Residual PP Removal of PS Component in Converted-Wave Seismic Reflection Processing, Scientific Contributions Oil and Gas Journal, Vol. 43 No 2, 2020.

Triyoso, W., Supriyono, S., Akbar, F. S., Oktariena, M., Lestari, S., Yusuf B.E. & Miraza, D., (2023), The 3D Seismic Survey Design of South Walio Offshore, Indonesia: Optimizing the 3D Survey Design Parameters, Scientific Contri- butions Oil and Gas Journal, Vol. 46 No. 2, 2023. DOI: https://doi.org/10.29017/SCOG.46.2.1552.

Wang, Y., 1999, Approximations to the Zoeppritz equations and their use in AVO analysis: Geophysics, 64, 1920-1927. https://doi.org/10.1190/1.1444698.

Wang, Y., 2017, Seismic Inversion: Theory & Application, 127-138, Wiley Blackwell. https://doi.org/10.1190/SEGJ2018-022.1

Zhang., 2010, Joint Inversion of Seismic PP- and PS-Waves in the Ray Parameter Domain, Imperial College London, 1-22.